Available online at www.sciencedirect.com
ScienceDirect
International Journal of Heat and Mass Transfer 51 (2008) 2090–2107
International Journal of HEAT and MASS TRANSFER
www.elsevier.com/locate/ijhmt

Temperature variations in the simulation of high-pressure injection-system transient flows under cavitation

A.E. Catania, A. Ferrari *, E. Spessa

Dipartimento di Energetica, Politecnico di Torino, Corso Duca degli Abruzzi, 24-10129 Torino, Italy

Received 12 March 2007; received in revised form 18 November 2007
Available online 11 February 2008

Abstract

Temperature variations and their effects on the simulation of unsteady pipe flows, in the presence of pressure-wave induced cavitation, were investigated with reference to high-pressure fuel injection systems. The thermal effects due to the compressibility of the liquid and to the thermodynamic process in the cavitating flow mixture were analyzed. To that end, the energy conservation equation was applied, in addition to the mass-continuity and momentum-balance equations, along with the constitutive state equation of the fluid. In particular, for the liquid, the physical properties (i.e., bulk modulus of elasticity, density, isothermal speed of sound, thermal expansivity, kinematic viscosity, specific heat at constant pressure) were implemented as functions of pressure and temperature in a closed analytical form matching carefully determined experimental data. Consistent with virtually negligible combined effects of heat transfer and viscous power losses involved in the flow process, the equation of energy was reduced to a state relation among the fluid thermodynamic properties, leading to a barotropic flow model. A comparison between isentropic and isothermal evolutions in the pure liquid regions was carried out for evaluating the influence of the temperature variation simulation on the macroscopic results given by local pressure time-histories. Besides, for cavitation analysis, different thermodynamic transformations of the vapor–liquid mixture were considered and compared.

A recently developed conservative numerical model of general application, based on a barotropic flow model, was applied and further assessed through the comparison of prediction and measurement results on injection-system performance.

A conventional pump-line-nozzle system was considered for this purpose, being relevant to model evaluation for its pressure-wave dynamics and also because it was subject to severely cavitating flow conditions at part loads. Predicted time-histories of injector-needle lift and pressure at two pipe locations were compared to experimental results. This substantiated the validity and robustness of the conservative model taking temperature variation effects into account, in the simulation of high-pressure injection-system transient flows with great degree of accuracy, even in the presence of cavitation induced discontinuities. The thermal effects due to the temperature variations in the liquid fuel and in the cavitating mixture were analyzed and discussed.

Keywords: Acoustic cavitation; Diesel injection systems; Temperature effects

1. Introduction

Mathematical modeling and numerical simulation have long been used as powerful tools for investigating the complex unsteady flow phenomena that occur in high-pressure fuel injection systems of both the conventional pump-line-nozzle and the new generation multiple injection types (e.g., [1–11]). Sophisticated numerical models are necessary to study the response of these systems to changes in design and operating variables, particularly when severely modified working conditions are imposed by drastic changes in the oil temperature. Besides, to prevent erosion damages that possible cavitation occurrence can induce, the model should also be capable of accurately predicting cavitating flow phenomena.

Transient flow simulation in high-pressure fuel injection systems has long been carried out with the hypothesis of isothermal flow [1–7]. However, temperature variations

* Corresponding author.
E-mail address: alessandro.ferrari@polito.it (A. Ferrari).

0017-9310/$ - see front matter © 2007 Elsevier Ltd. All rights reserved.
doi:10.1016/j.ijheatmasstransfer.2007.11.032

Nomenclature

a	speed of sound
A	flow area
$\mathbf{A}$	Jacobian matrix
c	specific heat along a polytropic evolution
d	pipe diameter
E	bulk modulus of elasticity
F	spring force
$\mathbf{F}$	physical flux vector
h	enthalpy per unit mass
$\mathbf{H}$	source vector
k	spring stiffness; ratio between constant-pressure and constant-volume specific heats
$\dot{l}_w$	viscous power dissipation per unit mass
L	length of pipe and injector-drilled passage
m	mass
p	pressure; average cross-sectional pressure
$\dot{q}$	heat transfer rate per unit mass
Q	volumetric flow-rate
s	entropy per unit mass
S	section
t	time
T	temperature
u	average cross-sectional velocity
v	specific volume or volume per unit mass
V	volume
$\mathbf{w}$	conservative variable vector
x	axial coordinate; air gap
α	void fraction
β	thermal expansivity; damping
Δt	time increment
Δx	distance increment
ζ	damping factor
θ	cam angle
μ	mass fraction; discharge flow coefficient
ξ	time increment ratio
ρ	density; average cross-sectional density
τ_w	wall shear stress
$\mathbf{\Phi}$	numerical flux vector

Subscripts

0	reference value; total enthalpy per unit mass
bs	seats
d	delivery outlet
i	injector inlet
in	chamber inlet
l	liquid
m	mobile element
M	maximum value
n	needle
out	chamber outlet
p	at constant pressure
T	at constant temperature
s	at constant entropy
v	vapor phase; at constant volume

due to the compressibility of the liquid fuel can play a significant role in injection-system modeling. In particular, such is the case when very high-pressure levels and remarkable wave propagation dynamics take place throughout relatively long pipes or when considerable changes in the environmental fluid temperature sensibly alter the physical properties of the fuel.

In [9–11] the authors took the liquid-fuel density dependence on temperature into account for accurately predicting pressure time-histories in both conventional and electronically-controlled high-pressure fuel injection systems.

Transient flows and acoustic cavitation, i.e., cavitation induced by pressure waves, were simulated by several numerical models, with various difficulty levels and accuracy degrees, in hydraulic systems [12–18].

A thermodynamic approach of general application to pipe-flow cavitation simulation was developed in [10], based on a simple, effective, conservative barotropic flow model. The proposed approach incorporated, as particular cases, the pseudo-cavitation [12–14,17–19], the pure vaporous and pure gaseous cavitations as well as the pure liquid flow, in addition to the vapor cavitation in the presence of a dissolved gas. A physically consistent isothermal evolution was considered for the homogeneous mixture of liquid and aeriform constituents in the pure vaporous-cavitation model.

Numerical methods used to solve pipe-flow equations, in addition to discretization procedures and resolution algorithms for injection-system mathematical modeling were surveyed in [5,10]. A thorough review of cavitating flow simulation approaches is reported in [10].

In the present work, compressibility induced temperature variations were predicted in the liquid fuel of a pump-line-nozzle diesel injection system. The nonstationary distributions of the fluid thermodynamic properties along the pressure pipes, including the injector-drilled passage, were analyzed in order to evaluate the so induced thermal effects in the simulation of these systems. For this purpose, the energy conservation equation was introduced and reduced to a state relation among the fluid intensive properties, in accordance with negligible overall effects of wall heat-transfer and viscous power losses involved in the flow. The constitutive state equation of the liquid fuel was used for closing the set of the model partial differential equations. To that end, the oil physical properties were expressed as analytic functions of pressure and temperature by fitting accurate experimental data [10] and were introduced in the numerical code.

With regard to cavitation simulation, different thermodynamic evolutions of the vapor–liquid mixture were considered, in addition to the isothermal process, so as to reduce the energy equation to a property state-relation in any case. Predicted pressure and void-fraction distributions under isentropic and isenthalpic processes were compared to those of an isothermal process.

Macroscopic thermal effects on pressure time-histories, due to the liquid fuel compressibility and to temperature variations during the cavitating mixture evolutions were assessed by comparing the prediction results to the experimental data taken in a conventional pump-line-nozzle diesel injection system, at partial and full loads. Such a system was of particular relevance to the flow model validation, including temperature variation effects due to: the remarkable wave propagation phenomena taking place in the particularly long system pressure-pipes, the relatively high values of the injection pressures at full load, and also the severely cavitating flow conditions the system was subjected to, at part loads.

2. Injection experimental system

The experimental data for model assessment were obtained in a high-pressure fuel injection system built by Bosch for medium-duty vehicles and made up of a pump of the in-line type, a relatively long pressure pipe and a single-spring injector. Measurements of the pressure time-histories at two pipe locations, one close to the pump outlet (p_d) and the other close to the injector inlet (p_i), were taken, along with the injector-needle lift (l_n), on a specifically instrumented test bench. The pump run at the angular speed of 1300 rpm and the pump governor control lever was kept in a partial-load position first, where sensibly cavitating pipe-flow conditions occurred and then in its full-load position. The pump-plunger strokes were determined for both lever positions. Ensemble-averaged pressure and lift data were taken. Pressures were gauged with piezoresistive transducers and the needle lift was acquired by means of an inductive transducer. The injection system was operated with the test-oil ISO 4113 that is ordinarily used to simulate diesel fuel. The oil was supplied to the pump at a temperature of ≈40 °C at part and full load operations. Fig. 1 shows a schematic of the injection-system layout, including the acquired quantities and measurement locations. Key geometrical–operational parameters of mechanical components, relevant to the numerical model [7], and also accurately measured oil properties were available.

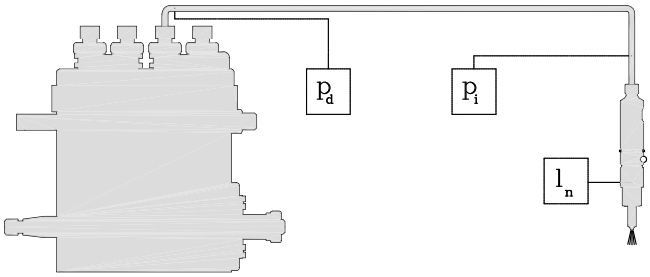

Fig. 1. Measurement system layout.

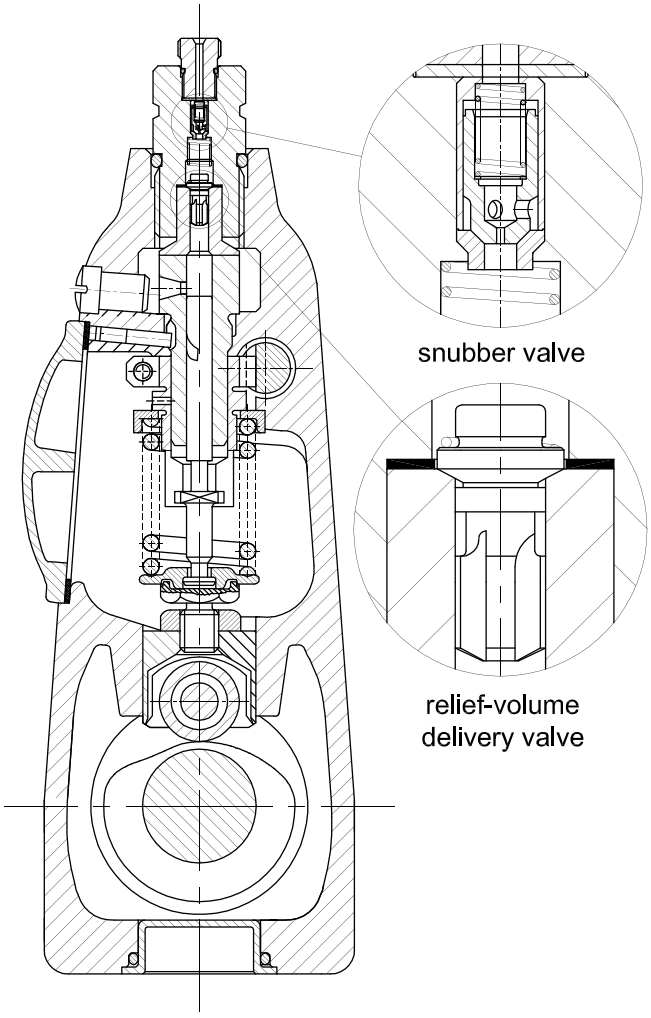

Fig. 2. In-line pump.

Fig. 2 shows the in-line pump with the delivery valve assembly. This was equipped with a valve of the relief-volume type, in order to avoid injector-nozzle reopening, and with a snubber valve for attenuating the possible cavitation occurrence inside the pipe [20]. The plunger-lift distributions, as well as the inlet- and spill-port cross-sectional areas, were also acquired as functions of the camshaft angle. Fig. 3 shows the single-spring injector presenting a nozzle of the orifice type with five holes and a reduced sac volume.

The delivery valve is open during the injection phase when the fluid flows from the pump to the injector. At the end of injection, consequent to the opening of the spill port by the pump plunger, the delivered flow motion reverts back to the pump. The relief-volume valve has a retraction collar, giving rise to a relief volume of 40 mm^3 in the back flow during the valve closure with the purpose of attenuating the back-flow pressure-wave

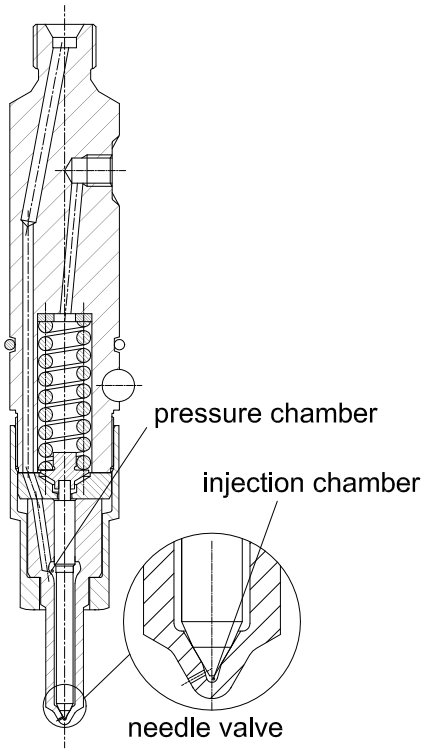

Fig. 3. Single-stage injector.

reflection at the delivery valve head after the valve closure, so as to avoid the possible injector-nozzle reopening. However, an excessively damped pressure-wave reflection can be undesirable in order to hinder the cavitation that may be caused by the depression wave subsequent to the spill port opening. The snubber valve reduces the depression wave harmful effects. In fact, when the spill port opens, the snubber valve closes, leaving only a small passage to the fluid flowing toward the delivery valve chamber. In this way a backpressure arises in the snubber-valve chamber so as to compensate for the relief-volume damping effect on the pressure-wave reflection. Thus, the cavitation occurrence can be prevented or attenuated although it may be still a remarkable phenomenon to be carefully taken into account.

3. Pressure pipe model

The pipe connecting the pump to the injector, or any transmission line in hydraulic systems, can be generally treated as a slender pipeline for which a one-dimensional flow model is suitable. The fluid flowing through the pressure pipe is modeled as a pure liquid in the absence of cavitation or outside regions under cavitation. Whenever the pressure decreases up to the vapor tension at local temperature, the fluid is modeled as a homogeneous no-slip mixture of liquid and vapor. In this case, the vapor is considered to be finely distributed within the cavitating regions or, more specifically, within each of the computational cells.

Following a conservative formulation, the pipe-flow model equations are written in the divergence form, that is, using a control volume approach for a pipe element with constant cross-section, the mass-conservation and momentum-balance equations can be expressed as follows:

$$\frac{\partial \mathbf{w}}{\partial t}+\frac{\partial \mathbf{F}}{\partial x}=\mathbf{H} \tag{1}$$

where

$$\mathbf{w}=\begin{bmatrix}\rho\\ \rho u\end{bmatrix},\quad \mathbf{F}(\mathbf{w})=\begin{bmatrix}\rho u\\ \rho u^2+p\end{bmatrix},\quad \mathbf{H}=\begin{bmatrix}0\\ -\frac{4\tau_w}{d}\end{bmatrix} \tag{2}$$

t is the time variable and x is the axial variable along the pipe; ρ, u and p are the average cross-sectional density, velocity and pressure, respectively, of either the liquid or the homogeneous mixture; d is the internal diameter of the pipe and τ_w is the wall (or boundary) shear stress, given by $\tau_w = f\rho|u|u/8$, f being the Darcy–Weisbach resistance coefficient [12]. Since the fluid density (ρ) and momentum (ρu) have been chosen as unknown variables, Eq. (1) can be applied both in the absence and in the presence of cavitation.

The conservation equations of only mass and momentum are generally adequate for mathematically modeling a compressible pure liquid flow or a homogeneous mixture of liquid and gaseous constituents under the hypothesis of isothermal evolution [1–7,12–16]. In such a case, being the temperature specified, the additionally required state equation reduces to $p = p(\rho)$.

In order to take account of the thermal effects due to the liquid-fuel compressibility and evaluate the effects of a specific thermodynamic process on the liquid vaporization under cavitation, the energy equation should be introduced. The total (thermal and mechanical) energy conservation equation can be written in the following divergence form:

$$\frac{\partial(\rho h_0-p)}{\partial t}+\frac{\partial(\rho h_0 u)}{\partial x}=\rho(\dot{q}+\dot{l}_w)-\frac{4\tau_w}{d}u \tag{3}$$

h_0 is the total (or stagnation) enthalpy per unit mass of the fluid system, i.e., $h_0 = h + u^2/2$, $\dot{q}$ is the heat transfer rate per unit mass from the boundaries to the system and $\dot{l}_w$ is the viscous power dissipation per unit mass within the system. Combining Eq. (3) with the continuity equation and with the following conservation equation of the mechanical energy (obtained multiplying by u each term of the momentum-balance equation)

$$\frac{1}{2}\rho\left(\frac{\partial u^2}{\partial t}+u\frac{\partial u^2}{\partial x}\right)=-u\left(\frac{\partial p}{\partial x}+\frac{4\tau_w}{d}\right) \tag{4}$$

one obtains:

$$\frac{\mathrm{d}h}{\mathrm{d}t}-\frac{1}{\rho}\frac{\mathrm{d}p}{\mathrm{d}t}=\dot{q}+\dot{l}_w \tag{5}$$

Introducing the entropy, Eq. (5) gives rise to the so called 'heat equation', i.e., the basic thermodynamic relation among the fluid state variables in any elemental process:

$$T\,\mathrm{d}s = \mathrm{d}h - \frac{\mathrm{d}p}{\rho} \tag{6}$$

where T is the local temperature and s is the entropy per unit mass of the system. If a thermodynamic process is specified for the fluid, Eq. (6) reduces to an equation among the state variables. Such equation and the state equation of the fluid $p = p(\rho, T)$ close the pipe-flow model Eq. (1), as will be specified for the two cases of pure liquid and cavitating flows.

3.1. Pure liquid flow

The pressure p is derived from the state equation of the liquid $p = p(\rho, T)$, which can be put in the following differential form [10]:

$$\mathrm{d}p = a_{\mathrm{T}}^2\,\mathrm{d}\rho + \beta E_{\mathrm{T}}\,\mathrm{d}T \tag{7}$$

where $a_{\mathrm{T}} = \sqrt{E_{\mathrm{T}}/\rho}$ is the speed of sound at constant temperature

$$\beta = \frac{1}{v}\left(\frac{\partial v}{\partial T}\right)_p = -\frac{1}{\rho}\left(\frac{\partial \rho}{\partial T}\right)_p \tag{8}$$

is the volumetric coefficient of thermal expansion or the thermal expansivity and

$$E_{\mathrm{T}} = -v\left(\frac{\partial p}{\partial v}\right)_{\mathrm{T}} = \rho\left(\frac{\partial p}{\partial \rho}\right)_{\mathrm{T}} \tag{9}$$

is the isothermal bulk modulus of elasticity of the fluid.

Eq. (7) explicitly introduces the temperature T as an additional variable. Thus, the further relation that is required to close the equation set can be obtained in the form of another state equation as follows. A virtually adiabatic flow and a negligible thermal effect of viscous dissipation can be considered, consistently with relatively small flow velocities, or rather a compensation can be assumed between the small heat-transfer and viscous loss effects. In such a case Eq. (6) yields the following thermodynamic relation among the fluid state variables:

$$\mathrm{d}h - \frac{\mathrm{d}p}{\rho} = 0 \tag{10}$$

For a simple system of fixed composition, as the pure liquid is, the enthalpy fundamental equation in differential form, arising from p, ρ, T, c_p and β information, can be easily verified to be [10]:

$$\mathrm{d}h = c_p\,\mathrm{d}T + (1 - \beta T)\frac{\mathrm{d}p}{\rho} \tag{11}$$

Thus, from Eqs. (10) and (11), taking $a_{\mathrm{T}} = \sqrt{E_{\mathrm{T}}/\rho}$ in mind, the following nondimensional equation is obtained linking pressure and temperature variations:

$$\frac{\mathrm{d}p}{E_{\mathrm{T}}} = \frac{c_p}{\beta a_{\mathrm{T}}^2}\frac{\mathrm{d}T}{T} \tag{12}$$

In the present work, this state equation was applied to evaluate the variations of the liquid temperature due to compressibility effects, for high-pressure injection-system simulation.

3.2. Cavitating flow

The fluid portion under cavitation can be treated as a macroscopically homogeneous and isotropic mixture of pure liquid and its vapor provided the amount of this latter is very small and its bubbles are finely distributed [5,10,15,17]. Generally, such is the case in high-pressure fuel injection systems, even at cavitating conditions that are considered to be severe for them [10]. Any arbitrarily small amount of dissolved gas was neglected, according to [5,10,17], although a general approach, including gaseous cavitation, was developed in [10]. The cavitating mixture is treated as a pure phase at a macroscopic level by considering average local intensive properties in it. In particular, a mechanical and thermodynamic equilibrium model results [5,12,17] by neglecting the surface tension and viscosity in the static bubble-wall equilibrium and taking a mass-averaged internal energy of the mixture, leading to an average local temperature that is virtually equal to the liquid temperature, due to the tiny amount of the vaporous component involved. Besides, if the tiny vapor bubbles are finely distributed, so that the mixture can be regarded as a homogeneous and isotropic system, no slip between liquid and aeriform constituents is reasonably assumed. In this case, the mass and void fractions of the vaporous phase are introduced as variables:

$$\mu = \frac{m_{\mathrm{v}}}{m} \quad \text{and} \quad \alpha = \frac{V_{\mathrm{v}}}{V} \tag{13}$$

where m_{v} and V_{v} indicate the vapor mass and volume, respectively, m and V designate the mass and volume of the mixture. The mass (μ) and the void (α) fractions are linked by the following relationship:

$$\mu = \frac{\rho_{\mathrm{v}}}{\rho}\alpha \tag{14}$$

If the intensive properties of the mixture so characterized are related by a thermodynamic statement describing the evolution it is subjected to (barotropic flow model), only one intensive property (namely ρ) is required to describe its internal state. In fact, the system has one degree of freedom according to the *Gibbs phase rule* [21].

Applying the primitive definition of specific volume to the mixture, as well as to each of its constituents, and introducing the mass fraction μ of the vapor phase Eq. (13), the homogeneous mixture density can be expressed in general as a function of the vapor and liquid densities as well as of the vapor mass fraction, by

$$\rho = \frac{\rho_{\mathrm{v}}\rho_{\mathrm{l}}}{\mu\rho_{\mathrm{l}} + (1 - \mu)\rho_{\mathrm{v}}} \tag{15}$$

The liquid and vapor densities in Eq. (15) are functions of p, that is, $\rho_{\mathrm{l}} = \rho_{\mathrm{l}}(p)$ and $\rho_{\mathrm{v}} = \rho_{\mathrm{v}}(p)$, because in the vapori-

zation regions the temperature T is a function of pressure, $T = T(p)$.

If the mixture density ρ is assumed as the property that describes the so attained monovariant system, then the vapor mass fraction μ must be a function of ρ. This indicates that Eq. (15) connects the pressure p to the density ρ of the mixture, as should be for a barotropic flow. Therefore, one can calculate the pressure gradient as follows:

$$\frac{\partial p}{\partial x} = \frac{\mathrm{d}p}{\mathrm{d}\rho}\frac{\partial \rho}{\partial x} \tag{16}$$

To obtain a general expression for the local speed of sound in the mixture, Eq. (1) is rewritten in the following quasi-linear form:

$$\frac{\partial \mathbf{w}}{\partial t} + \mathbf{A}\frac{\partial \mathbf{w}}{\partial x} = \mathbf{H} \tag{17}$$

where

$$\mathbf{A} = \begin{bmatrix} 0 & 1 \\ \frac{\mathrm{d}p}{\mathrm{d}\rho} - u^2 & 2u \end{bmatrix} \tag{18}$$

is the Jacobian matrix of the partial differential equation system. As can be easily verified, the eigenvalues λ of the matrix $\mathbf{A}$ are

$$\lambda_{1,2} = u \pm \sqrt{\frac{\mathrm{d}p}{\mathrm{d}\rho}} \tag{19}$$

so that the local speed of sound in the mixture results to be

$$a = \sqrt{\frac{\mathrm{d}p}{\mathrm{d}\rho}} \tag{20}$$

in accordance with the thermodynamic definition of sound speed for a fluid subjected to a specific evolution law.

From Eq. (20), taking the derivative of ρ (Eq. (15)) with respect to the pressure p, the following analytical relation is obtained for the sound speed in the cavitating mixture:

$$\frac{1}{\rho a^2} = \frac{\alpha}{\rho_\mathrm{v} a_\mathrm{v}^2} + \frac{1-\alpha}{\rho_\mathrm{l} a_\mathrm{l}^2} - \rho\left(\frac{1}{\rho_\mathrm{v}} - \frac{1}{\rho_\mathrm{l}}\right)\frac{\mathrm{d}\mu}{\mathrm{d}p} \tag{21}$$

where a_v, a_l are the sound speeds of constituents for the specific thermodynamic process. The first two terms on the right hand side of Eq. (21) are related to the elasticity properties of each component of the mixture, whereas the last term refers to the vaporization or condensation process, as can also be easily verified by working out the definition of an effective bulk modulus of elasticity for the mixture [10].

It should be pointed out that different authors [12,14,17–19] neglect the last term in Eq. (21) and use the following expression for the mixture speed of sound, with reference to any vaporous or gaseous constituent (denoted by the subscript g):

$$\frac{1}{\rho a^2} = \frac{\alpha}{\rho_\mathrm{g} a_\mathrm{g}^2} + \frac{1-\alpha}{\rho_\mathrm{l} a_\mathrm{l}^2} \tag{22}$$

Actually, Eq. (22) refers to a two-phase mixture whose cavities contain a fixed amount of an indissoluble and incondensable gas. Therefore, bubbles can grow or decrease in response to changes of the liquid pressure without any mass transfer across the bubble surface. Such a sound speed model was referred to as pseudo-cavitation in [10,22]. The limits and approximations in the application of Eq. (22) to pipe-flow acoustic cavitation simulation are analyzed in [22].

The knowledge of the derivative $\frac{\mathrm{d}\mu}{\mathrm{d}p}$ is required to obtain the local speed of sound a from Eq. (21). Thus, combining Eqs. (6), (11) and (14) with the following expression of the mixture enthalpy increment:

$$\mathrm{d}h = r\,\mathrm{d}\mu + \mu\,\mathrm{d}h_\mathrm{v} + (1-\mu)\mathrm{d}h_\mathrm{l} \tag{23}$$

one obtains:

$$T\,\mathrm{d}s = r\,\mathrm{d}\mu + c_p\,\mathrm{d}T - \left[\frac{1}{\rho} - \frac{1-\mu}{\rho_\mathrm{l}}(1-\beta_\mathrm{l}T)\right]\mathrm{d}p \tag{24}$$

where the subscripts v and l refer to the vapor and liquid, respectively, c_p is the average specific heat of the mixture at constant pressure, defined by

$$c_p = \mu c_{p_\mathrm{v}} + (1-\mu)c_{p_\mathrm{l}} \tag{25}$$

ρ is the mixture density, given by Eq. (14), $r = r(T)$ is the vapor condensation heat.

Eq. (24) and the specification of the thermodynamic process allow modeling the vapor source term, i.e., the derivative of μ with respect to the pressure p. In particular, for an *isentropic process* ($\mathrm{d}s = 0$), Eq. (24) yields:

$$r\frac{\mathrm{d}\mu}{\mathrm{d}p} = \left[\frac{1}{\rho} - \frac{1-\mu}{\rho_\mathrm{l}}(1-\beta_\mathrm{l}T)\right] - c_p\frac{\mathrm{d}T}{\mathrm{d}p} \tag{26}$$

whereas, for an *isenthalpic process* ($\mathrm{d}h = 0$) one has

$$r\frac{\mathrm{d}\mu}{\mathrm{d}p} = -\frac{1-\mu}{\rho_\mathrm{l}}(1-\beta_\mathrm{l}T) - c_p\frac{\mathrm{d}T}{\mathrm{d}p} \tag{27}$$

Finally, if the assumption of *isothermal process* ($\mathrm{d}T = 0$) is made for the cavitating region, the pressure assumes the constant value of the vapor tension at the specified temperature there, so that ρ_v and ρ_l are determined. Thus, Eq. (15) directly relates the vapor mass fraction μ to the mixture density ρ, so that the increment of μ is related to the mixture density variation by

$$\mathrm{d}\mu = -\frac{\rho_\mathrm{v}\rho_\mathrm{l}}{\rho_\mathrm{l} - \rho_\mathrm{v}}\frac{d\rho}{\rho^2} \tag{28}$$

Since μ takes variable nonnegative values, its derivative with respect to p tends to infinite. Thus, Eq. (21) leads to $a = a_\mathrm{T} \to 0$ which means that in effect the sound speed of the fluid under the isothermal cavitation process is negligibly small.

In the present work, an isothermal evolution was selected to simulate the cavitating flow, on the ground of:

the tiny vaporizing liquid amount; the simplicity and accuracy of such evolution in capturing macroscopical effects; the conservativeness of it in the vapor amount prediction with respect to isentropic or isenthalpic processes, as will be shown further on. Therefore, in the vapor–liquid mixture under cavitation, the pressure and temperature keep at constant values, whereas the mixture density is still variable and is numerically calculated by solving the system of Eq. (1). The ρ value thus obtained was used to work out the void fraction

$$\alpha = \frac{\rho_l - \rho}{\rho_l - \rho_v} \tag{29}$$

As a result, during cavitation the compressibility of the mixture is related to the phase change, rather than to the elastic properties of the fluid.

3.3. Effect of pipe wall elasticity

Considering the elastic properties of the pipe material, one can take the fluid-structure interaction into account by introducing the effective bulk modulus E_{eff} and sound speed a_{eff} as follows:

$$\frac{1}{E_{\text{eff}}} = \frac{1}{\rho a_{\text{eff}}^2} = -\frac{1}{V}\frac{\mathrm{d}V}{\mathrm{d}p} - \frac{1}{V}\frac{\mathrm{d}V_{\text{pipe}}}{\mathrm{d}p} \tag{30}$$

where V is the fluid volume and V_{pipe} the volume delimited by the internal pipe diameter. In agreement with Eq. (21), one can set:

$$\frac{1}{\rho a^2} = -\frac{1}{V}\frac{\mathrm{d}V}{\mathrm{d}p} \tag{31}$$

Substitution of Eq. (31) into Eq. (30) leads to the following relation:

$$\frac{1}{\rho a_{\text{eff}}^2} = \frac{1}{\rho a^2} - \frac{1}{V}\frac{\mathrm{d}V_{\text{pipe}}}{\mathrm{d}p} \tag{32}$$

The second term on the right hand side of Eq. (32) takes the pipe elasticity effects into account. From stress and strain considerations, for a thin-walled pipe one obtains [5]:

$$-\frac{1}{V}\frac{\mathrm{d}V_{\text{pipe}}}{\mathrm{d}p} = C \cdot \frac{d}{E_p \cdot e} \tag{33}$$

where E_p is the Young modulus of elasticity of the pipe material, d is the pipe internal diameter, e is the pipe wall thickness and C is a constraint factor, which depends on the support conditions of the pipe. According to Eqs. (30)–(33), the effective sound speed a_{eff} decreases with respect to a when the ratio of d/e increases and thus the stiffness of the transmission line reduces. For d/e lower than 5, as in the present case, the pipe is not considered to be thin-walled and the contribution of the term $1/V \cdot \mathrm{d}V_{\text{pipe}}/\mathrm{d}p$ to the value of a_{eff} is drastically reduced. The commercial high-pressure pipe of an in-line-pump diesel fuel-injection system can have d/e ratios between 2 and 1.5. Consequently, the effect of the fuel-line elasticity on the oil speed of sound is negligible, so that it is possible to set $a_{\text{eff}} \approx a$ [5].

4. Pump and injector

The pressure-wave propagation along the injector-drilled passages was simulated by the foregoing pipe-flow model, whereas a lumped mass model was applied to write the continuity equations for the pump and injector isobaric chambers. Further details on the rebuilt injection-system model are given in [23].

The chambers are numbered according to the model of Fig. 4, so that, with reference to a generical chamber j, one can write:

$$Q_{\text{in},j} - Q_{\text{out},j} = \frac{1}{\rho_j}\frac{\mathrm{d}\rho_j}{\mathrm{d}t}V_j + \frac{\mathrm{d}V_j}{\mathrm{d}t} \tag{34}$$

where for $j = 1, 2, 3, 5$ the volumetric flow-rate coming into the chamber j is given by

$$Q_{\text{in},j} = \frac{p_{j-1} - p_j}{|p_{j-1} - p_j|}\mu_{\text{in},j}A_{\text{in},j}\sqrt{\frac{2}{\rho_j}|p_{j-1} - p_j|} \tag{35}$$

and for $j = 1, 2, 4, 5$ the volumetric flow-rate going out of the chamber j is given by

$$Q_{\text{out},j} = \frac{p_j - p_{j+1}}{|p_j - p_{j+1}|}\mu_{\text{out},j}A_{\text{out},j}\sqrt{\frac{2}{\rho_j}|p_j - p_{j+1}|} \tag{36}$$

Valve flow coefficients were taken according to [7], whereas for the injector nozzle holes unsteady flow coefficients were used, on the basis of specific experiments [24,25]. It should be pointed out that $Q_{\text{out},3}$ and $Q_{\text{in},4}$ were regarded as variables at the boundaries of the pipe including the injector-drilled passage.

The valve dynamics (the injector needle is also referred to as the nozzle valve) were simulated according to a second-order linear-system model, as illustrated in Fig. 5:

$$m_{\text{m}}\frac{\mathrm{d}^2 l_{\text{m}}}{\mathrm{d}t^2} + \bar{\beta}_{\text{m}}\frac{\mathrm{d}l_{\text{m}}}{\mathrm{d}t} + \bar{k}_{\text{m}}l_{\text{m}} + \bar{F}_0 = \sum_k p_k S_{m_k} \tag{37}$$

where

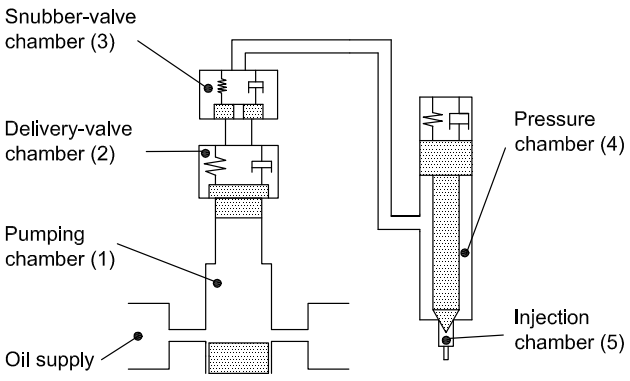

Fig. 4. Model of pump and injector.

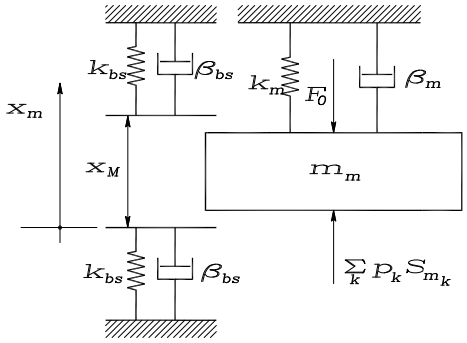

Fig. 5. Second-order dynamics model for valves.

$$
\begin{aligned}
&l_{\mathrm{m}} < 0, \quad \bar{k}_{\mathrm{m}} = k_{\mathrm{m}} + k_{\mathrm{bs}}, \quad \bar{\beta}_{\mathrm{m}} = \beta_{\mathrm{m}} + \beta_{\mathrm{bs}}, \quad \bar{F}_0 = F_0,\\
&0 \leqslant l_{\mathrm{m}} \leqslant l_M, \quad \bar{k}_{\mathrm{m}} = k_{\mathrm{m}}, \quad \bar{\beta}_{\mathrm{m}} = \beta_{\mathrm{m}}, \quad \bar{F}_0 = F_0,\\
&l_{\mathrm{m}} \geqslant l_M, \quad \bar{k}_{\mathrm{m}} = k_{\mathrm{m}} + k_{\mathrm{bs}}, \quad \bar{\beta}_{\mathrm{m}} = \beta_{\mathrm{m}} + \beta_{\mathrm{bs}},\\
&\bar{F}_0 = F_0 - k_{\mathrm{bs}} \cdot l_M
\end{aligned}
$$

with

$$\beta_{\mathrm{m}} = 2\zeta_{\mathrm{m}}\sqrt{k_{\mathrm{m}} m_{\mathrm{m}}} \tag{38}$$

5. ISO 4113 oil properties

The physical properties (i.e., bulk modulus of elasticity, density, isothermal speed of sound, thermal expansivity, kinematic viscosity, specific heat at constant pressure) of the test-oil ISO 4113, simulating the diesel fuel, are reported in Figs. 6–11, as dependent variables of pressure and temperature. More specifically, the properties are expressed by analytical functions of the pressure p, taking the temperature T as parameter. The figures compare the experimental data (symbols) to the model equations (solid lines) that were implemented in the numerical code.

The isothermal bulk modulus of elasticity is accurately described by the following empirical linear equation:

$$E(p,T) = E_{\mathrm{T}}(p) = E_0(T) + \chi(T)(p - p_0) \tag{39}$$

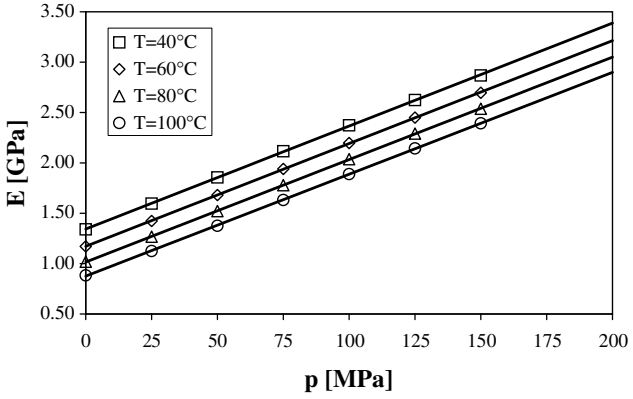

Fig. 6. Bulk modulus of elasticity: comparison between experimental data (symbols) and Eq. (39) results (solid lines).

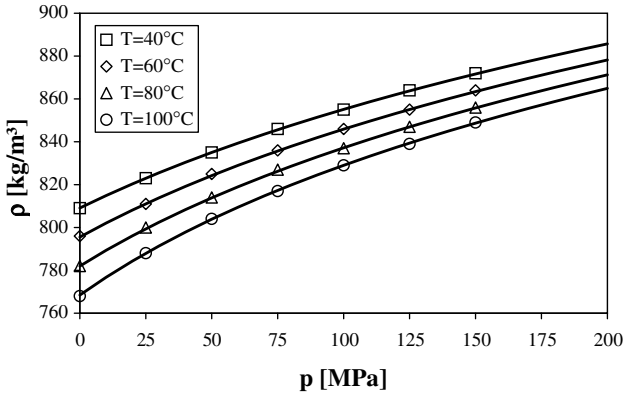

Fig. 7. Density: Eq. (41) results (solid lines) versus experimental data (symbols).

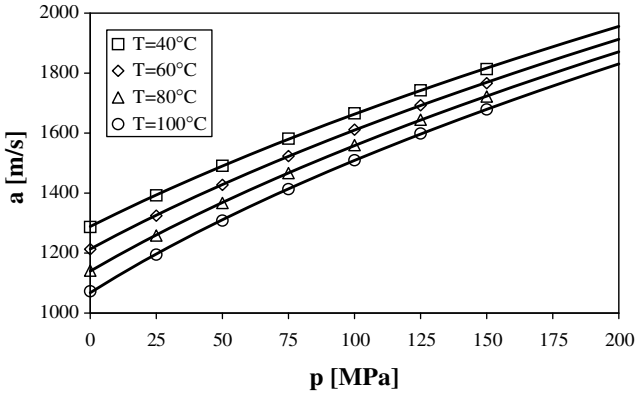

Fig. 8. Isothermal speed of sound: Eq. (42) (solid lines) versus experimental results (symbols).

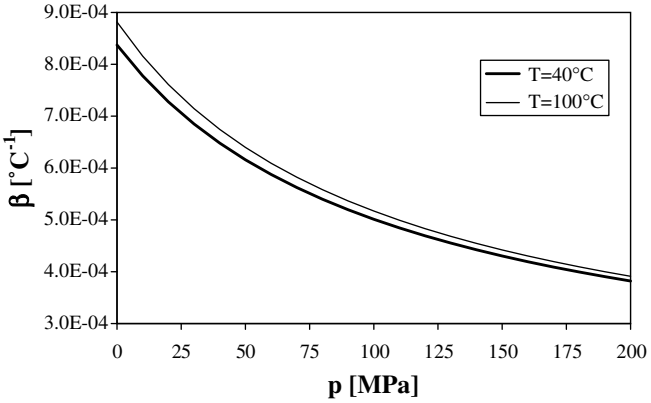

Fig. 9. Thermal expansivity.

where p_0 is a reference pressure, $E_0(T)$ is the value of the liquid elasticity modulus at pressure p_0 and temperature T. The analytical relations $E_0(T)$ and $\chi(T)$ are reported in [23]. A plot of Eq. (39) and of experimental data at four temperatures in the range of interest for the present study is given by Fig. 6.

In order to obtain the relation between the oil density and pressure, let us start from the definition of the bulk elasticity modulus of Eq. (9), which gives

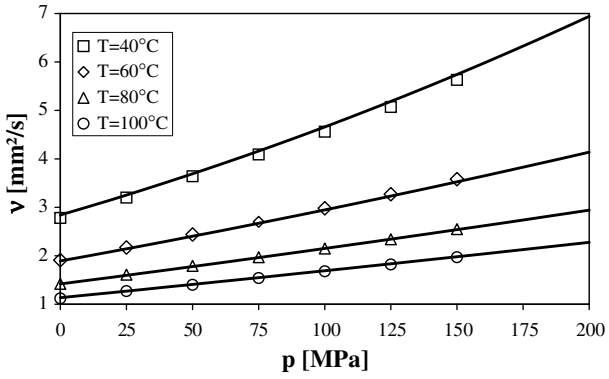

Fig. 10. Kinematic viscosity: Eq. (44) (solid lines) versus experimental results (symbols).

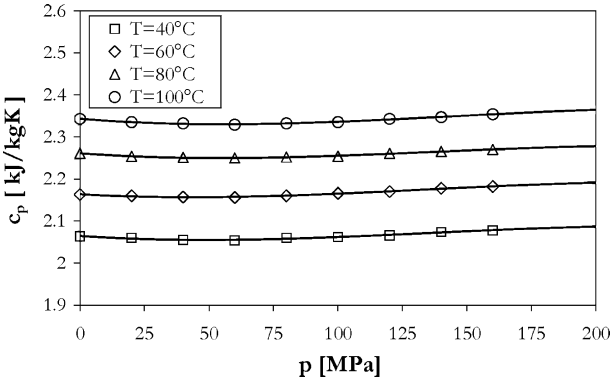

Fig. 11. Specific heat at constant pressure: comparison between experimental (symbols) and analytical (Eq. (45)) results.

$$\left(\frac{\partial p}{\partial \rho}\right)_{\mathrm{T}} = \frac{E_{\mathrm{T}}(p)}{\rho} \tag{40}$$

A direct integration of this equation yields

$$\rho(p,T) = \rho_{\mathrm{T}}(p) = \rho_0(T)\left[\frac{E_{\mathrm{T}}(p)}{E_0(T)}\right]^{\frac{1}{\chi(T)}} \tag{41}$$

where $\rho_0(T)$ is the liquid density value at $p = p_0$, as a function of T [23]. The density distributions versus pressure are plotted in Fig. 7 for the indicated temperatures.

The isothermal sound speed of the liquid, as a function of pressure and temperature, is given by

$$a(p,T) = a_{\mathrm{T}}(p) = \sqrt{\frac{E_{\mathrm{T}}(p)}{\rho}} \tag{42}$$

The comparison between Eq. (42) outcome and measurement data is presented in Fig. 8, showing again a very good agreement between analytical and experimental results.

The volumetric coefficient of the liquid thermal expansion

$$\beta(p,T) = -\frac{1}{\rho}\left(\frac{\partial \rho}{\partial T}\right)_p \tag{43}$$

was determined by differentiation of Eq. (41) with respect to the temperature. A slight dependence of β on temperature is shown in Fig. 9, plotting β versus pressure at 40 °C and 100 °C.

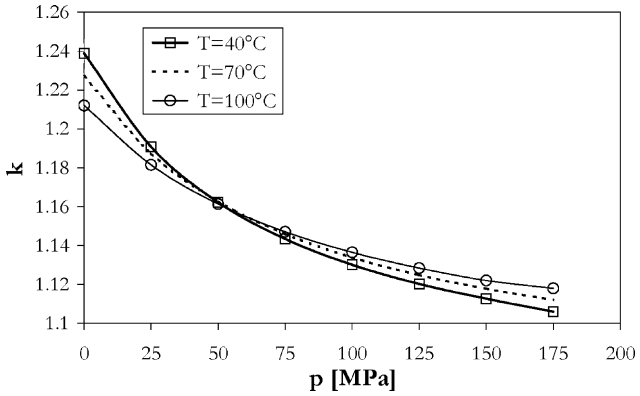

Fig. 12. Ratio between c_{p} and c_{v}.

A good analytical expression for the oil kinematic viscosity (Fig. 10) is provided by the following quadratic polynomial:

$$v(p,T) = \eta_0(T) + \eta_1(T)p + \eta_2(T)p^2 \tag{44}$$

where η_0, η_1, η_2 are power functions of the temperature [23].

The specific heat at constant pressure of the test oil is very well approximated by the following cubic expression:

$$c_p(p,T) = c_0(T) + c_1(T)p + c_2(T)p^2 + c_3(T)p^3 \tag{45}$$

in which c_0, c_1, c_2, c_3 are growing quadratic functions of the temperature T, fitting the measured data. The agreement of Eq. (45) results with experimental data is presented in Fig. 11.

Fig. 12 plots the ratio k of the specific heat at constant pressure to that at constant volume, expressed by

$$k = \frac{c_p}{c_{\mathrm{v}}} = \left[1 - \frac{(\beta a_{\mathrm{T}})^2}{c_p}\cdot T\right]^{-1} \tag{46}$$

as a function of the pressure p at different temperatures T. The values of k have been worked out by Eq. (46) using Eqs. (42), (43) and (45). As can be inferred from Fig. 12, for liquid fluids k assumes smaller values than those that are typical of gaseous flows. Nevertheless, it is always sensibly different from unity. From Eqs. (45) and (46) one can calculate c_{v} as a function of p and T.

6. Numerical algorithm and solution

A new finite-volume scheme was proposed to discretize the system of hyperbolic partial differential equations, given by Eq. (1). It is an implicit, conservative, one-step, symmetrical and trapezoidal scheme of the second-order accuracy, which will also be referred to by the acronym ICOST (Implicit Conservative One-step Symmetric Trapezoidal scheme [10,23]). Consistent with a finite-volume approach [26,27], the ICOST scheme can be expressed in the form:

$$\mathbf{w}_j^{n+1} = \mathbf{w}_j^n - \frac{\Delta t}{\Delta x}\left(\mathbf{\Phi}_{j+\frac{1}{2}}^{n+\frac{1}{2}} - \mathbf{\Phi}_{j-\frac{1}{2}}^{n+\frac{1}{2}}\right) + \Delta t \mathbf{H}_j^{n+\frac{1}{2}} \tag{47}$$

where the subscript j refers to the spatial grid locations, the superscript n designates the time level, $\mathbf{\Phi}$ is the numerical flux function defined as

$$\mathbf{\Phi}_{j+\frac{1}{2}}^{n+\frac{1}{2}} = \frac{1}{2}(\mathbf{F}_{j+1}^n + \mathbf{F}_j^n) - \frac{1}{2}\left(\frac{\Delta t}{\Delta x}\right)\left[\mathbf{A}_{j+\frac{1}{2}}^{n+1}(\mathbf{F}_{j+1}^{n+1} - \mathbf{F}_j^{n+1})\right]$$

$$\mathbf{\Phi}_{j-\frac{1}{2}}^{n+\frac{1}{2}} = \frac{1}{2}(\mathbf{F}_j^n + \mathbf{F}_{j-1}^n) - \frac{1}{2}\left(\frac{\Delta t}{\Delta x}\right)\left[\mathbf{A}_{j-\frac{1}{2}}^{n+1}(\mathbf{F}_j^{n+1} - \mathbf{F}_{j-1}^{n+1})\right]$$

$\mathbf{A}$ is the Jacobian matrix of the flux vector $\mathbf{F} = \mathbf{F}(\mathbf{w})$ (Eq. (18)).

At the pipe boundaries, upwind schemes were applied on the basis of characteristic considerations.

From the Von Neumann stability analysis of the ICOST difference approximation to the linear wave equation, it follows that the proposed scheme can be considered to be unconditionally stable. Thus, it was possible to select the mesh sizes Δt and Δx paying specific attention to accuracy requirements. In order to prevent numerical oscillations around discontinuities, second-order schemes usually introduce flux limiters [26,27], but the high-resolution schemes so obtained are more cumbersome to apply than those without limiters are. In the present work, the implementation of the high-resolution version of the ICOST scheme [23] does not involve differences in the simulation of the macroscopic effects with respect to the case without limiters. In particular, as will be shown by the results (Figs. 16 and 17b), in the presence of flow discontinuities induced by cavitation inception and desinence, no significant oscillation problems were caused by the ICOST scheme. On the other hand, available nonoscillatory schemes are either of the explicit type or too onerous to apply to injection systems, or are nonconservative [7,27–29]. Nevertheless, nonconservative schemes can yield satisfactory results at a macroscopic level, by properly handling the numerical solution of the split equations for the liquid and cavitating regions [5,7], particularly when slightly cavitating flows occur.

The choice of an implicit scheme is motivated in what follows. To discretize the ordinary differential equations modeling pump and injector dynamics, BDF (Backward Differentiation Formulas) of the second-order accuracy were used, being suitable for problems of the stiff type [5,10]. At each time step the primitive variables ρ, u, were derived from the conservative variables ρ, ρu, used to discretize Eq. (1) in both cases of the presence and absence of cavitation. In order to determine also the variables p and T, for the pure liquid flow Eq. (1) was solved conjunctly with the state Eqs. (7) and (12). For the cavitating flow, the state equation $p = p_v(T)$ was used to close Eq. (1) in the isothermal approach, p_v being the vapor pressure at temperature T. In the case of isentropic or isenthalpic evolutions, Eq. (15), taking $p = p_v(T)$, was applied for closure in conjunction with Eq. (26) or (27), respectively. A robust and accurate numerical algorithm was attained, capable of matching the nonstationary pipe fluid-dynamics to the dynamics of mechanical components at pipe boundaries.

7. Results

The predicted performance of the in-line pump injection system, in terms of needle lift distribution and pressure time-histories at two pipe locations, one close to the pump delivery outlet and the other close to the injector inlet, are given in Fig. 13 for two engine loads at the same pump speed of 1300 rpm [10]. The numerical results (solid line) are compared to the experimental data (circle symbol). The camshaft angle ($\theta - \theta_0$) is reported as abscissa, θ_0 being a reference angle.

The good agreement between computed and measured quantities evidenced by these results shows a quite satisfactory accuracy degree of the injection-system mathematical model including thermal effects.

Fig. 13a–c illustrate the injection-system performance at part load. Fig. 13a displays a sensible cavitation occurrence at the pipe inlet (pump delivery). The liquid pressure reaches the vapor-tension value at the cam angle $\theta - \theta_0 \approx 11°$ and keeps very low until the pressure wave coming back from the injector sweeps out the region under cavitation, increasing the pressure there. The fluid leaves the tiny pressure conditions at $\theta - \theta_0 \approx 19°$. As can be inferred from this figure, the model is capable of predicting with a good accuracy the duration of the very small pressure event and the intensity of the subsequent pressure peaks. This substantiates the validity of the conservative model for simulating wave propagation phenomena in the presence of cavitation.

The pressure peak in Fig. 13b has a higher value than that of the previous figure because it is affected by an accumulation effect due to the flow area reduction in the injector-drilled passage. Besides, due to the wave propagation with the compressibility driven sound speed, the pressure peak shows a time delay with respect to that of Fig. 13a. The comparison in Fig. 13c further validates the injector model, where the needle valve is treated as a second-order linear system. The small oscillations arising when the needle reaches its maximum lift and when the needle closes are due to the impact of the mobile element against the basement. No reopening of the needle valve is observed.

Fig. 13d–f shows the comparison between numerical and experimental results at full load. In Fig. 13d and e the pressure peaks present higher values than those of the corresponding diagrams at partial load, because of the greater pump-plunger useful stroke. The temporal delay of the pressure peak in Fig. 13e with respect to the peak in Fig. 13d is smaller than the corresponding one shown by Fig. 13b and a. This is due to the prevailing effect of the substantially higher pressure levels at full load, being the sound speed an increasing function of the pressure (Fig. 8). Besides, although cavitation occurs also at full load, it is not so intense and diffuse as at part load.

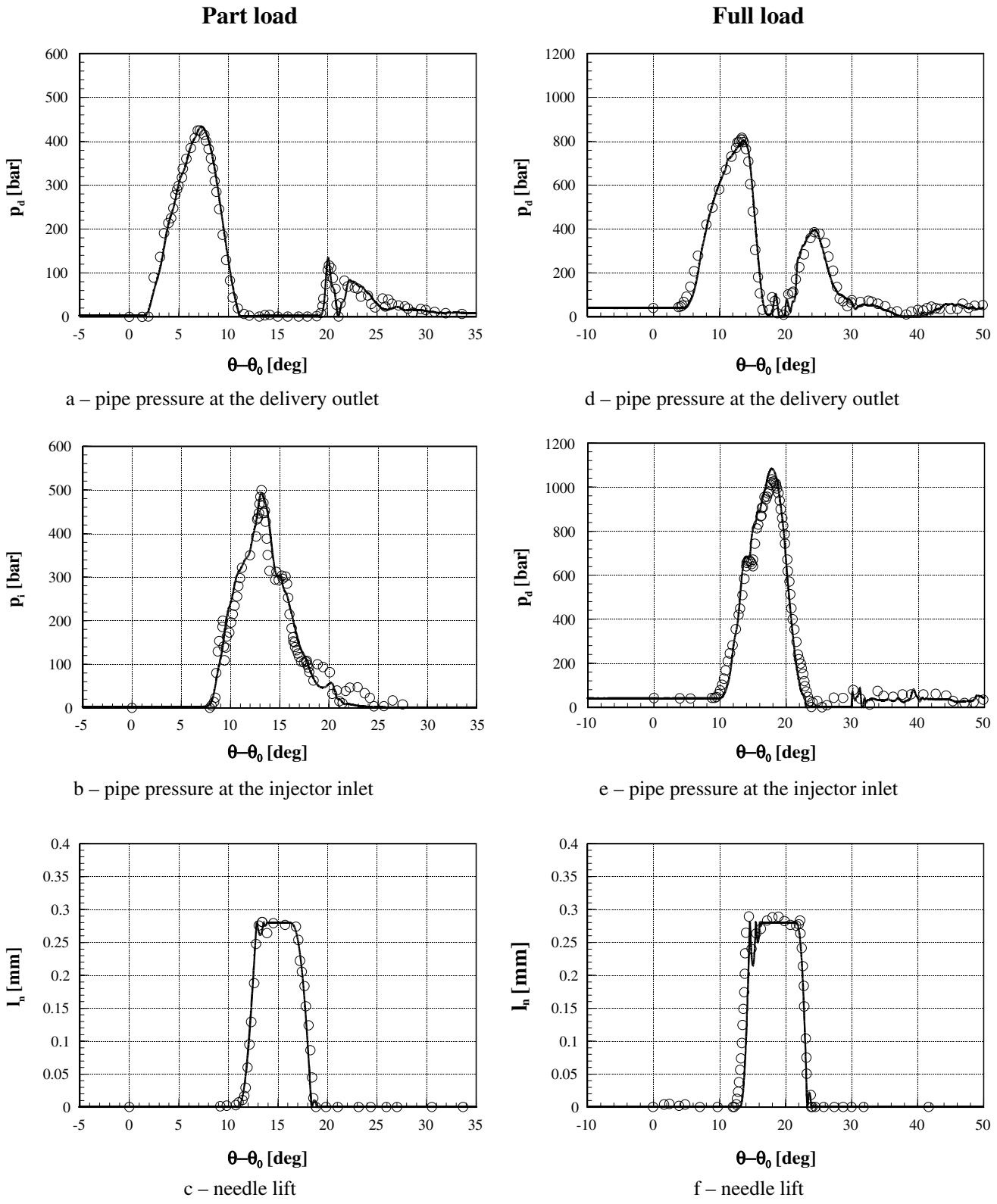

Fig. 13. Comparison between numerical and experimental results.

Fig. 14 shows a comparison between isentropic- and isothermal-flow simulations for both part and full loads at the same pump speed as above. It is worth pointing out that the pressure wave propagation in the pure liquid flow is closer to an isentropic event rather than to an isothermal one. Actually, a compression of nearly 400 bar leads to an increase of the oil temperature of more than 5 °C. The solid lines in Fig. 14 match those reported in Fig 13. The

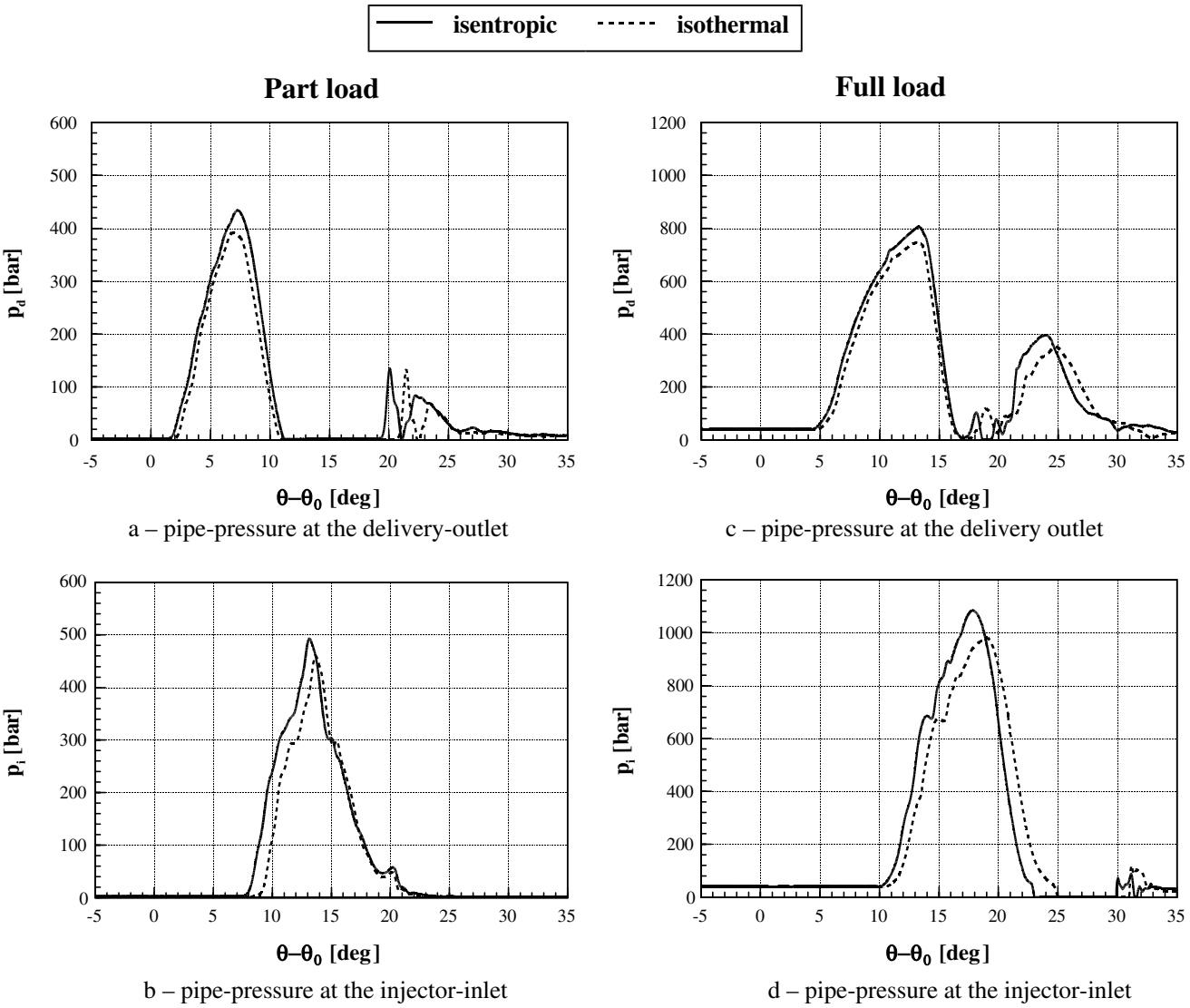

Fig. 14. Comparison between isentropic and isothermal evolutions.

dashed lines in Fig. 14 were obtained at the initial-temperatures of the fluid, i.e., ≈46 °C at part load and ≈58 °C at full load.

As can be inferred from Fig. 14, if temperature variations in the liquid are neglected, at measurement locations an estimation error in the pressure peak of nearly 50 bar can occur at part load (Fig. 14a and b) and of roughly 90 bar at full load (Fig. 14c and d). By comparison of the isentropic and isothermal results in the injector pressure chamber (not reported here), differences of up to 70 bar and of up to 120 bar were observed at part load and at full load, respectively. Moreover, the lower pressure levels of the isothermal evolution take account of the slower wave propagation motion, which causes the delay shown by the dashed lines with respect to the solid lines. However, it should be pointed out that small thermal effects were perceived in previous injection-system isothermal-flow predictions with respect to experimental results. This could be ascribed to the lower pressure levels and to the relatively short connecting pipes in the pump-line-nozzle systems which were considered [7].

Fig. 15 reports significant sequences of flow-property distributions along the pipe at full load, illustrating wave propagation phenomena for an isentropic (Fig. 15a) and an isothermal (Fig. 15b) evolution of the pure liquid flow. The abscissa reports the distance from the pump outlet, normalized to the length (L) of the connecting pipe and of the injector-drilled passage. The plots show pressure, flow-rate and temperature distributions along the pipe at different instants of time, corresponding to the indicated cam-angle coordinates $\theta - \theta_0$. As can be easily inferred from results at $\theta - \theta_0 = 13.5°$, the isothermal evolution corresponds to a delay in wave propagation due to lower values of the isothermal sound speed with respect to the isentropic one $a_s = \sqrt{k} a_T$ [10].

Fig. 16 plots sequences of flow properties (namely, pressure, temperature and void fraction) along the pipe at full load in the presence of cavitation. At a pipe location close

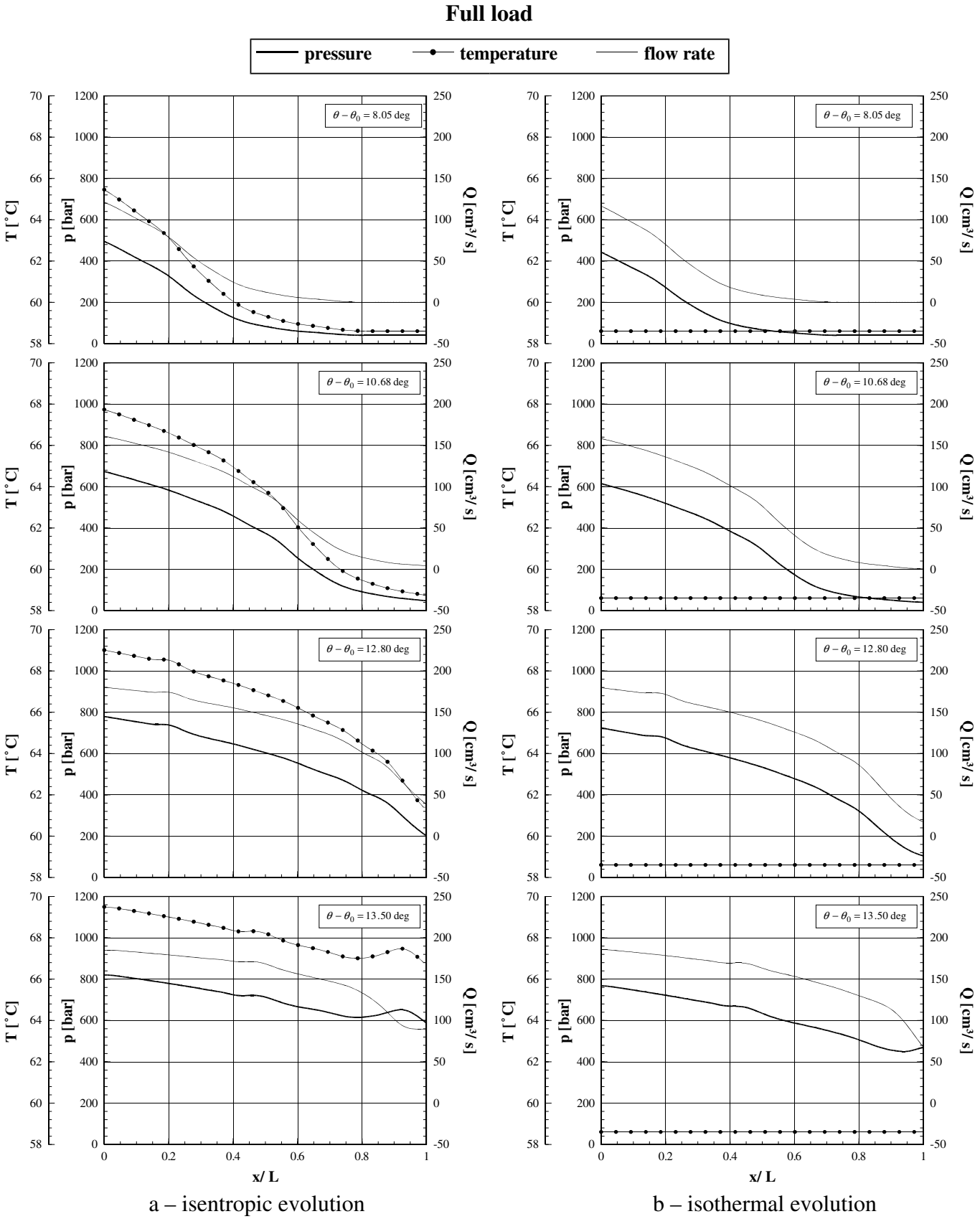

Fig. 15. Pure liquid flow.

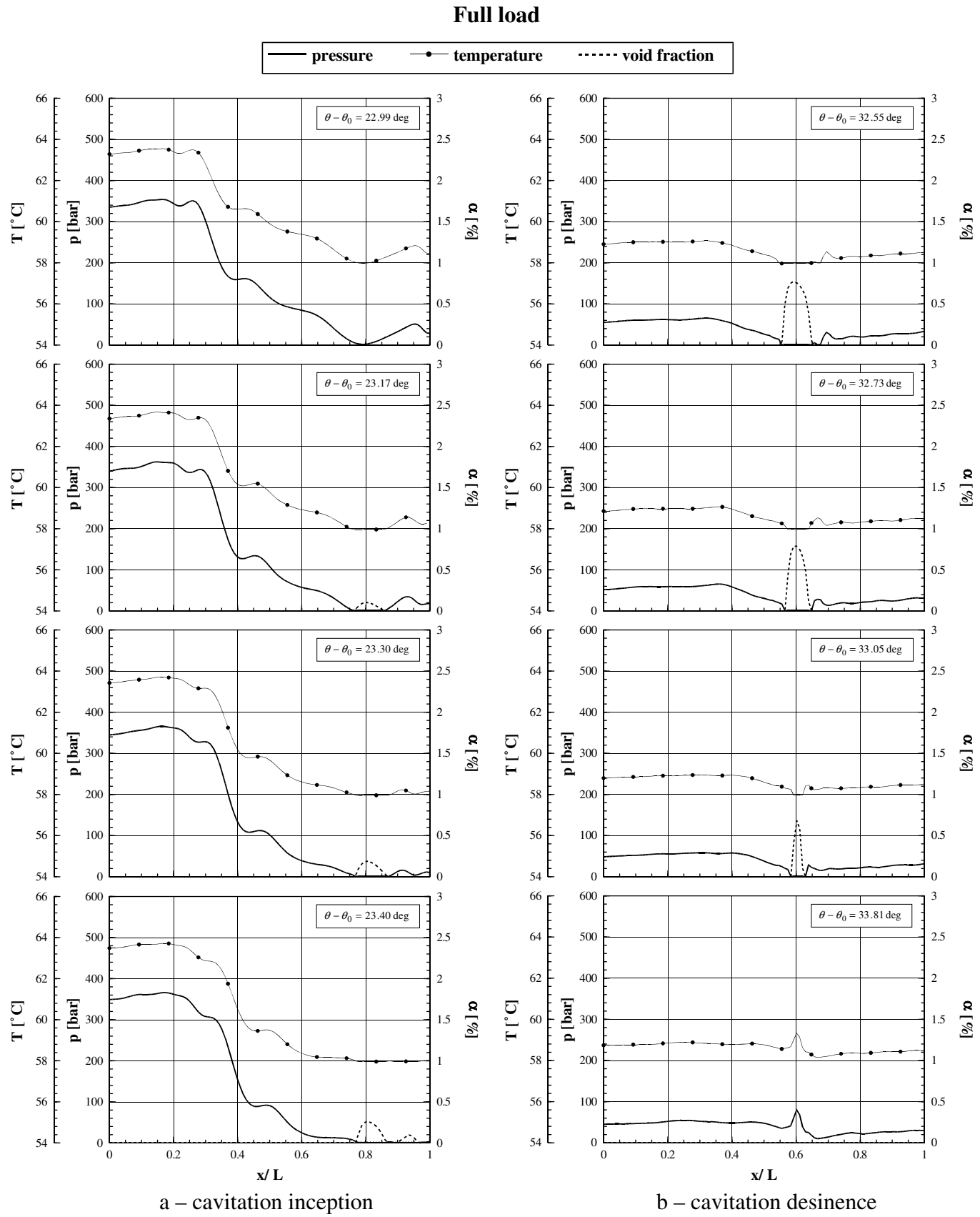

Fig. 16. Flow evolution along the pipe in the presence of cavitation.

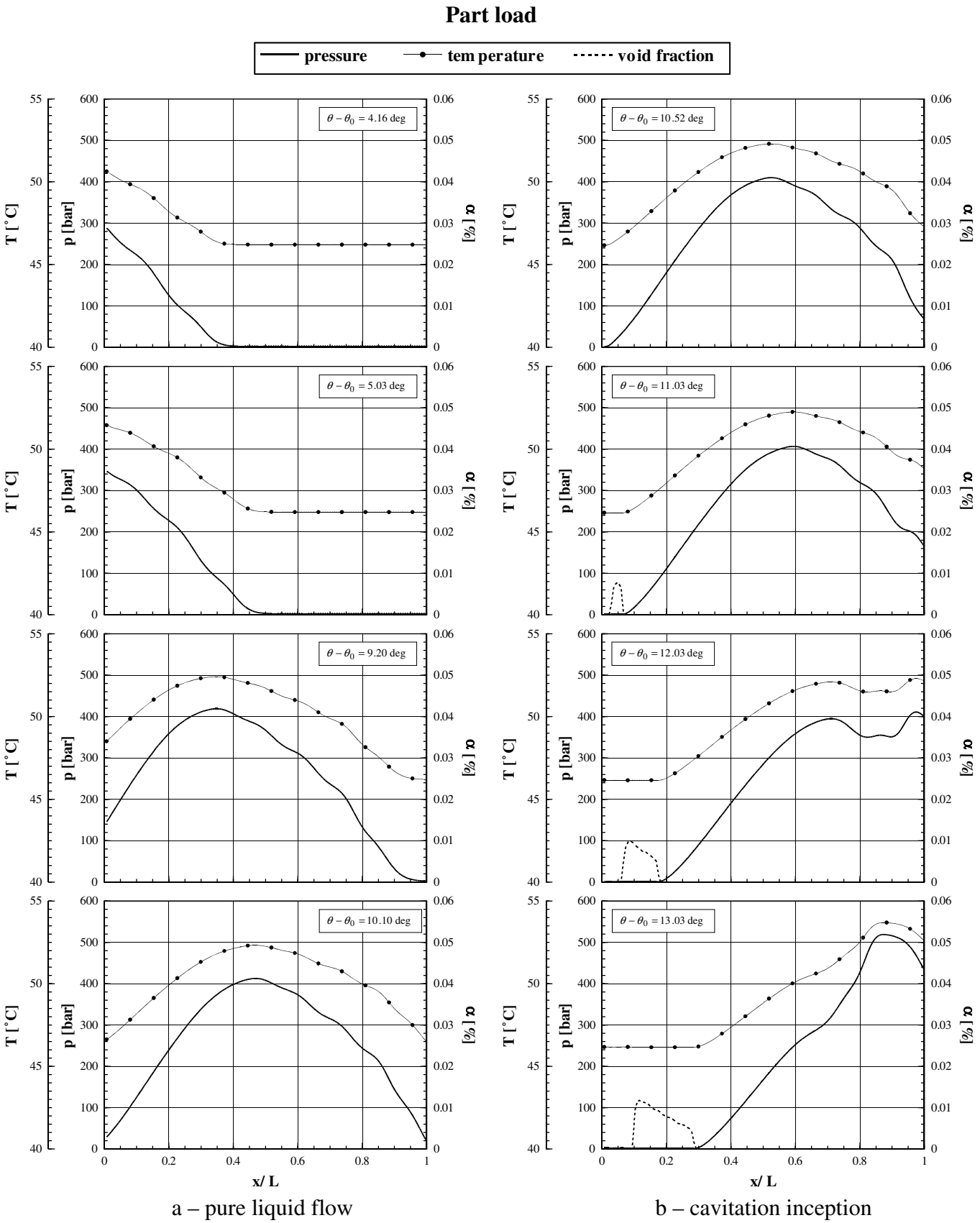

Fig. 17. Flow evolution along the pipe, in the absence (a) and presence (b) of cavitation.

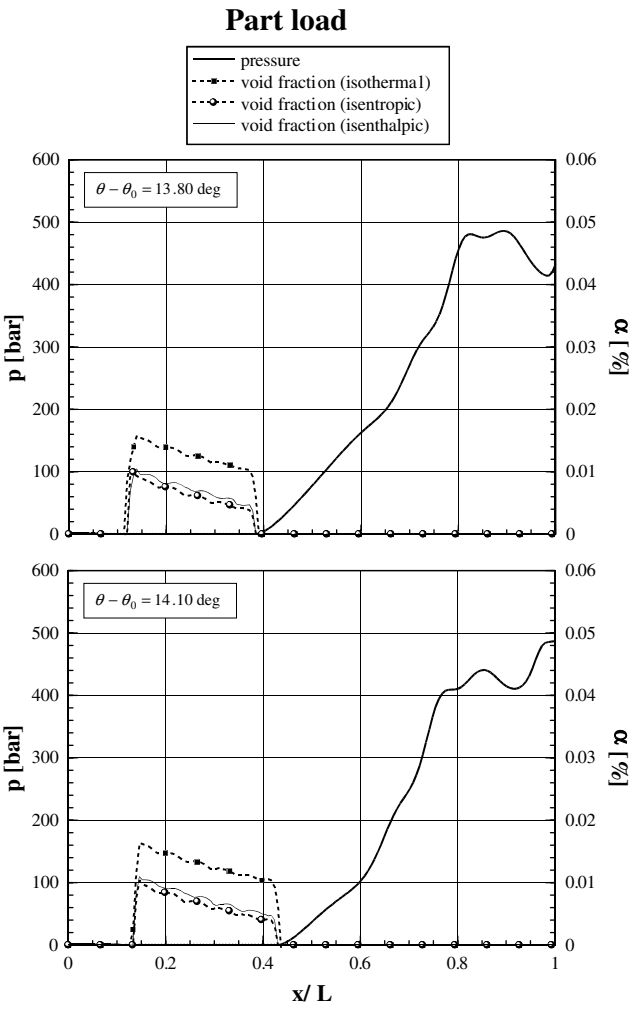

Fig. 18. Comparison between different models of cavitation evolution.

to the injector, Fig. 16a shows the cavitation inception caused by a rarefaction wave subsequent to the end of the injection phase. An interesting case of cavitation collapse is illustrated in Fig. 16b, where the void fraction in the cavitation region is swept away by pressure waves coming from both sides of this region. Because of the presence of two colliding flows, pressure and temperature peaks arise in the cavitation region when this disappears. This is illustrated by the last picture in Fig. 16b. As previously mentioned, during cavitation an isothermal process was considered, so that both temperature and pressure keep constant throughout the cavitating region, as is shown in Fig. 16. Two surfaces of discontinuity, separating the liquid from the cavitating regions, are visible in Fig. 16b. These discontinuities can be identified as shocks. In fact, the sound speed drops from the value a_l to zero across the discontinuities towards the cavitation region. Thus the supersonic flow existing at a pipe location inside such a region becomes subsonic when a liquid pressure wave crosses that location. Consequently, a shock takes place [10]. However, in Fig. 16a there is no evidence of any shock occurrence, because the subsonic flow at a certain pipe location becomes supersonic when such a location is reached by the cavitation. Therefore, a rarefaction wave is observed, instead of a shock.

Fig. 17 reports the flow-property distributions along the pipe for the same pump speed of 1300 rpm, but at part load. More specifically, Fig. 17a shows the pure liquid flow after the opening of the pump delivery valve and before the start of the injector-needle lift, whereas Fig. 17b illustrates the inception and subsequent evolution of cavitation during the rising of the needle valve up to its maximum lift. The rarefaction wave responsible for the cavitation occurrence is caused by the spill-port opening.

Fig. 18 shows the thermal effects that are related to the different thermodynamic evolutions the vapor mixture undergoes in the cavitation simulation. For the pure liquid flow, an isentropic process was assumed in all the cases that are shown in the figure, whereas inside the cavitating region three different transformations, that is, isothermal, isentropic and isenthalpic processes, were simulated for comparison.

The specific thermodynamic transformation of the vapor–liquid mixture gives rise to differences in the predicted void-fraction amount; in particular the void-fraction values obtained under the isothermal flow hypothesis were larger than the values resulting from the assumption of isenthalpic and isentropic transformations. It is worth pointing out that for the isenthalpic evolution higher values of the void fraction were found with respect to the isentropic one, according to the results obtained in simple pipeline test cases by other authors [17]. This is consistent with the patterns of these thermodynamic processes in the two-phase region of the *T-s* diagram for a pure substance.

Furthermore, the isentropic and isenthalpic evolutions produce very similar results because, close to the liquid saturation curve, these transformations are virtually similar in a very small range of pressure variations.

However, owing to the very small amount of vaporizing liquid usually involved in cavitation phenomena, such diversity in the computed void-fraction amounts does not affect the evolution of the other variables (pressure, flow-rate and temperature) in the surrounding liquid zones.

8. Conclusion

Temperature variations and their effects on the simulation of transient flows in high-pressure fuel injection systems were evaluated for both flow cases of pure liquid and of vapor–liquid mixture under acoustic cavitation, i.e., pressure-wave induced cavitation. More specifically, the thermal effects due to the compressibility of the liquid fuel and to the particular thermodynamic evolution of the cavitating mixture were analyzed.

A recently developed conservative numerical model of general application to both liquid and homogeneous two-phase flows, based on a barotropic flow model, was used and assessed at a macroscopic level by comparing predicted and experimental results on a diesel pump-line-nozzle injection-system performance.

The temperature variations associated either to the compressibility of the liquid fuel or to the cavitating region evolution, were computed by applying the thermal energy conservation equation. Consistent with negligible or globally compensating effects of the wall heat transfer and viscous power losses involved in the flow process, the energy equation was reduced to a state relation among the fluid thermodynamic properties, leading to the barotropic flow model. The numerical results indicated that temperature variations in the pure liquid flow can play a sensible role in the accuracy of transient-flow simulations within high-pressure injection systems. In fact, such thermal effects influenced the prediction of pressure peaks amplitude and therefore also the speed of the traveling waves with the consequence of shifts in the local pressure time-histories. Such effects are so more important as higher the pressures and the pipe lengths are.

With reference to cavitation simulation, different thermodynamic evolutions of the vapor–liquid mixture were considered, in addition to the isothermal process, so that the energy equation reduced to a state-relation among the fluid properties in any case. In particular, the macroscopic effects of isentropic and isenthalpic processes on pressure distributions were compared to those of an isothermal process.

It was shown that the specific thermodynamic evolution selected for cavitation modeling does not play a major role on the macroscopic results of the injection-system simulation. Actually, the pressure distributions are not significantly influenced by the variations in the void fraction produced by the different evolutions. Thus, an isothermal process was chosen because it is physically consistent with negligible temperature variations related to the tiny vaporizing liquid amount, and it is also very simple to be numerically handled. Besides, an isothermal transformation was shown to be the most conservative one with reference to the highest amount of void fraction production.

The second-order accurate conservative numerical scheme proposed to discretize the PDE system modeling the pipe flow proved to be capable of simulating the wave motion with a great accuracy degree, even in the presence of cavitation induced discontinuities. The developed mathematical model is capable of analyzing unsteady flows using the same hyperbolic equations both in the absence and in the presence of cavitation.

Acknowledgements

Financial support to this research was provided by Fiat Research Center and by MUR (Ministry of University and Research) under the COFIN 2004 Program.

References

[1] E.B. Wylie, J.A. Bolt, M.F. El-Erian, Diesel fuel injection system simulation and experimental correlation, SAE Paper No. 710569, 1971.

[2] S. Matsuoka, K. Yokota, T. Kamimoto, M. Igoshi, a study of fuel injection systems in diesel engines, SAE Paper No. 760551, 1976.

[3] K. Kumar, M.K. Gajendra Babu, R.R. Gaur, R.D. Garg, A finite difference scheme for the simulation of a fuel injection system, SAE Paper No. 831337, 1983.

[4] D.H. Gibson, A flexible fuel injection system simulation, SAE Paper No. 861567, 1986.

[5] A.E. Catania, C. Dongiovanni, A. Mittica, Implicit numerical model of a high-pressure injection system, ASME Trans. J. Eng. Gas Turb. Power 114 (1992) 534–543.

[6] C. Arcoumanis, M. Gavaises, E. Abdul-Wahab, V. Moser, Modeling of advanced high-pressure fuel injection systems for passenger car diesel engines, SAE 1999, Trans. J. Eng. 108 (2000) 1347–1362.

[7] A.E. Catania, C. Dongiovanni, E. Spessa, Delivery-valve effects on the performance of an automotive diesel fuel-injection system, SAE 1999, Trans. J. Eng. 108 (2000) 1399–1415.

[8] D.P. Schmidt, C.J. Rutland, M.L. Corradini, P. Roosen, O. Genge, Cavitation in two-dimensional asymmetric nozzle, SAE 1999, Trans. J. Eng. 108 (2000) 613–629.

[9] A.E. Catania, A. Ferrari, M. Manno, Development and application of a complete multijet common-rail injection system mathematical model for hydrodynamic analysis and diagnostics, ASME Paper ICES2005-1018, ASME Trans. J. Eng. Gas Turb. Power, in press.

[10] A.E. Catania, A. Ferrari, M. Manno, E. Spessa, A comprehensive thermodynamic approach to acoustic cavitation simulation in high-pressure injection systems by a conservative homogeneous two-phase barotropic flow model, ASME Trans. J. Eng. Gas Turb. Power 128 (2006) 434–445.

[11] A.E. Catania, A. Ferrari, E. Spessa, Numerical–experimental study and solutions to reduce the dwell time threshold for fusion-free consecutive injections in a multijet solenoid-type C.R. systems, ASME Paper ICES2006-1369, ASME TECHNICAL PAPER AWARD for best ICES2006 paper, ASME Trans. J. Eng. Gas Turb. Power, submitted for publication.

[12] M.H. Chaudhry, S.M. Bhallamudi, C.S. Martin, M. Naghash, Analysis of transient pressures in bubbly, homogeneous, gas–liquid mixtures, ASME Trans. J. Fluids Eng. 112 (1990) 225–231.

[13] J.-J. Shu, K.A. Edge, C.R. Burrows, S. Xiao, Transmission line with vaporous cavitation, ASME Paper No. 93-WA/FPST-2, 1993.

[14] T. Hapke, H.-K. Iben, Kavitationsmodellierung bei Eindimensional Strömungsvorgängen, Motortech Z., 1998.

[15] H. Nguyen-Schaefer, H. Sprafke, Numerical study on interaction effects of bubbles induced by air-release and cavitation in hydraulic systems, Tenth Bath International Fluid Power Workshop, Research Studies Press, John Wiley and Sons, New York, 1998.

[16] M. Beck, U. Iben, N. Mittwollen, H.-K. Iben, C.-D. Munz, On solution of conservation equations in cavitated hydraulic pipelines, in: Third International Symposium on Computational Technologies for Fluid/Thermal/Chemical Systems with Industrial Applications, July 22–26, Atlanta, GA, 2001.

[17] U. Iben, F. Wrona, C.D. Munz, M. Beck, Cavitation in hydraulic tools based on thermodynamic properties of liquid and gas, ASME Trans. J. Fluids Eng. 124 (2002) 1011–1017.

[18] W. Wallis, One dimensional Two-Phase Flow, McGraw Hill, New York, 1975.

[19] N.I. Kolev, Transiente Zweiphasen Strömung, Springer-Verlag, Berlin, 1986.

[20] R. Bosch, GmbH, Diesel-engine management, Bosch Technical Books, SAE International, 1999.

[21] A. Bejan, Advanced Engineering Thermodynamics, John Wiley and Sons, Inc., New York, 1997.

[22] A. Ferrari, A. Mittica, M. Manno, Cavitation analogy to gasdynamic shocks: model conservativeness effects on the simulation of transient flows in high-pressure pipelines, ASME Trans. J. Fluids Eng., in press.

[23] A. Ferrari, Development of a model for thermo-fluid dynamic transient simulation in high-pressure injection systems. Equipment of a high-performance test bench for diesel fuel injection systems: First Experimental Results on Common Rail System Dynamics, in Italian, Ph.D. thesis, Politecnico di Torino, 2004.
[24] A.E. Catania, C. Dongiovanni, A. Mittica, M. Badami, F. Lovisolo, Numerical analysis versus experimental investigation of a distributor-type diesel fuel-injection system, ASME Trans. J. Eng. Gas Turb. Power 116 (1994) 814–830.
[25] A.E. Catania, C. Dongiovanni, A. Mittica, C. Negri, E. Spessa, 1997, Experimental evaluation of injector-nozzle-hole unsteady flow-coefficients in light duty diesel injection systems, in: Proceedings, Ninth International Pacific Conference on Automotive Engineering 'Motor Vehicle and Environment', SAE-Indonesia, IPC-9 PRICE PAPER AWARD from SAE-Indonesia, vol. 1, pp. 283–290.
[26] C. Hirsch, Numerical computation of internal and external flows, Computational Methods for Inviscid and Viscous Flows, vol. 2, John Wiley and Sons, New York, 1988.
[27] R.J. LeVeque, Numerical Methods for Conservation Laws, Birkhäuser Verlag, Berlin, 1990.
[28] M.H. Chaudhry, M.Y. Hussaini, Second-order accurate explicit finite-difference schemes for waterhammer analysis, ASME Trans. J. Fluids Eng. 107 (1985) 523–529.
[29] A. Harten, B. Engquist, S. Osher, S.R. Chakravarthy, Uniformly high order accurate essentially non-oscillatory schemes III, J. Comput. Phys. 71 (1987) 231–303.